1998-08-01

Evaluation of personal communications dual-antenna handset diversity performance

Michael A. Jensen
jensen@byu.edu

Joseph S. Colburn

Yahya Rahmat-Samii

Gregory J. Pottie

Original Publication Citation

Colburn, J. S., et al. "Evaluation of Personal Communications Dual-Antenna Handset Diversity Performance." Vehicular Technology, IEEE Transactions on 47.3 (1998): 737-46

Evaluation of Personal Communications Dual-Antenna Handset Diversity Performance

Joseph S. Colburn, *Student Member, IEEE,* Yahya Rahmat-Samii, *Fellow, IEEE,*
Michael A. Jensen, *Member, IEEE,* and Gregory J. Pottie, *Member, IEEE*

***Abstract*—In personal wireless communications systems, multipath propagation has a significant effect on system design and performance. Signal strength fading caused by destructive interference between multiple replicas of the signal of interest arriving at the receiver over different paths often is the limiting factor in system range/fidelity. Antenna diversity is one technique that can be used to help overcome multipath fading. This paper presents a description of experiments, data processing, and results used to evaluate the diversity performance of three candidate dual-antenna handset configurations: two side-mounted planar-inverted F antennas (PIFA's), a back-mounted PIFA with a top-mounted helix, a top-mounted PIFA, and a "flip" monopole. In particular, the indoor industrial, scientific, and medical (ISM) band (902–928 MHz) propagation channel was of interest. These experiments did not include operator proximity effects, and in these tests, the dual-antenna handset remained stationary while the transmitter was moved along predetermined indoor paths. The issue of data normalization for extraction of fast fading behavior from measured data will be addressed, with results showing its effect on observed correlation presented. Also, measured indoor fading distributions are presented and seen to fit the Rician and Rayleigh models well. From the diversity results presented, it is seen that the three proposed dual-antenna handsets yield sufficient decorrelation to warrant consideration for use in diversity systems.**

***Index Terms*—Antenna diversity, correlation coefficient, handset antennas, multipath fading.**

I. Introduction

IN THE CELLULAR communications environment, short-term or fast fading due to multipath has a significant impact on the overall system performance. This type of fading occurs when multiple replicas of the signal of interest arrive at the receiver over different paths, thus having different relative amplitudes and phases. The total signal at the receiver is a vector summation of all these individually arriving replicas, the result being an interference pattern which usually contains significant signal fades. One technique to mitigate these short-term fades is diversity combining in which the signals received over different channels are combined properly to increase the probability the received signal is of adequate strength [1], [2]. Antenna diversity is one possible realization of this, where multiple antennas are used to provide the separate channels.

This paper summarizes the measured diversity performance of three dual-antenna handset configurations proposed for a cellular transceiver handset [7], [8] for the industrial, scientific, and medical (ISM) band: two side-mounted planar-inverted F antennas (PIFA's), a back-mounted PIFA with a top-mounted helix, a top-mounted PIFA, and a "flip" monopole. The diversity performance of these antenna geometries is assessed by determining the power correlation coefficient of the signals simultaneously measured over each of the two antennas located on the handset. In addition to the three dual-antenna handsets, as a reference the diversity experiments were performed on two dipole antennas with 0.06λ and 0.4λ element separation.

In this paper, considerable attention is given to the data-processing aspects of the diversity evaluation. The different measures of diversity performance are reviewed and related. Effort is also directed at the issue of data normalization and its effect on observed correlation. Finally, fading characteristics of the indoor environment studied are presented and compared to the Rayleigh and Rician distributions.

II. Antenna Configurations

The intent of this study was to evaluate the diversity performance of three dual-antenna configurations for a small transceiver handset. Fig. 1 illustrates the configurations considered: (a) top-mounted helix and back-mounted PIFA, (b) side-mounted PIFA's, and (c) top-mounted PIFA and "flip" monopole. The overall dimensions of the handset geometry considered are given in Fig. 1(c), with the specific antenna locations and dimensions for each design specified in Fig. 1(a)–(c).

Antenna diversity is accomplished by receiving the signal of interest with multiple antennas which have different reception characteristics, thus, the waveforms received by each antenna are somewhat decorrelated. Note that the effective transmission path for each channel in an antenna diversity system is an integration of the geometric and diffraction ray paths with the pattern/polarization characteristics of the transmit and receive antennas. The difference in reception characteristics between the antennas can be achieved by variation in the polarization, pattern and spatial location of the antennas [9], [10]. Different field components are affected differently by the same surroundings, thus, polarization can be used to achieve some level of decorrelation. Antennas with different patterns or

Manuscript received November 1, 1995; revised November 18, 1996. This work was supported by ARPA under Contract DAAB07-93-C-C501.

J. S. Colburn, Y. Rahmat-Samii, and G. J. Pottie are with the Department of Electrical Engineering, University of California, Los Angeles, CA 90095-1594 USA.

M. A. Jensen is with the Department of Electrical and Computer Engineering, Brigham Young University, Provo, UT 84602-4099 USA.

Publisher Item Identifier S 0018-9545(98)05866-6.

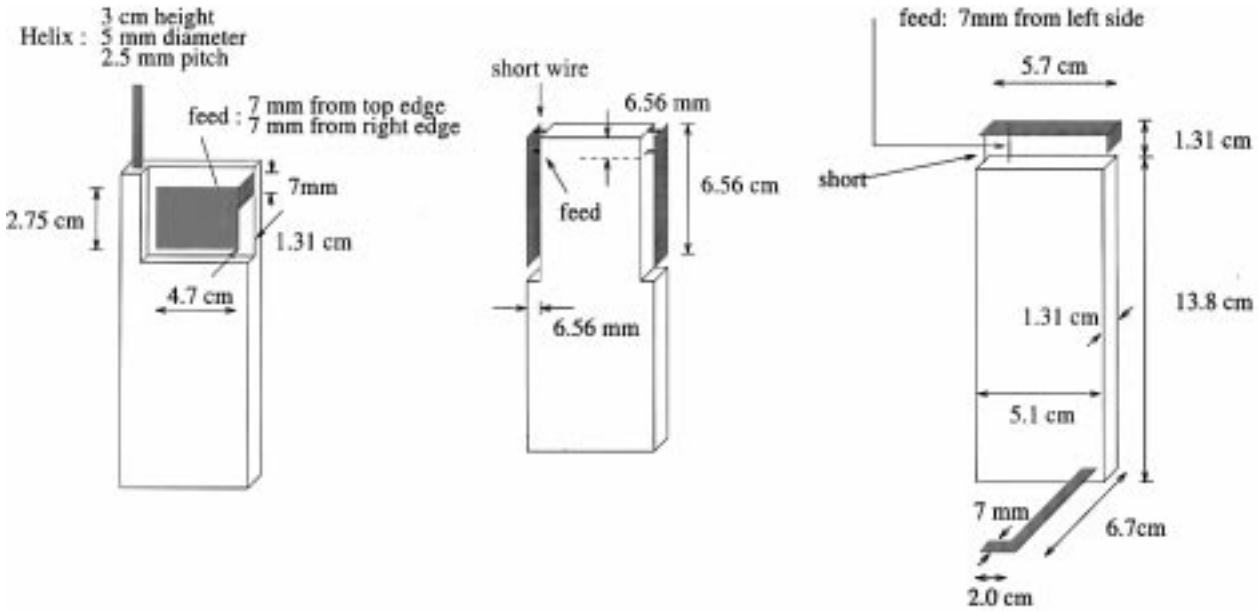

Fig. 1. Handset antenna configurations considered: (a) top-mounted helix and back-mounted planar-inverted F (PIFA), (b) side-mounted PIFA's, and (c) top-mounted PIFA and "flip" monopole.

identical antennas with different orientations achieve decorrelation because they receive over different effective paths. Also, by merely displacing two antennas, their effective receive paths will be different, resulting in some decorrelation between the signals received by the two antennas.

The dual-antenna handsets illustrated in Fig. 1 achieve their overall diversity performance from all three types of antenna diversity: spatial, polarization, and pattern. Consider the top-mounted helix and back-mounted PIFA structure shown in Fig. 1(a). These two antennas are displaced from each other ($\approx$ 5 cm) and have different pattern and polarization characteristics, resulting in significant decorrelation between the two received signals. Similarly, the dual-side-mounted PIFA configuration illustrated in Fig. 1(b) also achieves pattern and polarization diversity through physical element displacement as well as opposite orientation. These same descriptions also apply to the top-mounted PIFA and "flip" monopole handset of Fig. 1(c) although in this case a significantly larger element separation is used ($\approx$15 cm).

All the antennas, except the helix, were simulated on the handset using a finite-difference time-domain (FDTD) computer program prior to construction to analyze their performance [7], [8]. The design goal was to achieve better than a 2 : 1 voltage-standing wave ratio (VSWR) over the 902–928-MHz bandwidth in addition to good diversity performance. During construction, the structures were modified as required to achieve the optimal impedance match.

III. Data Processing

A. Correlation Coefficients

In this work, the measure of diversity performance of the proposed antenna configurations used is the power correlation coefficient between the signals received over the two antennas mounted on the handset. The correlation coefficient is a commonly used gauge of diversity and has three different forms: complex signal (ρ_s), envelope (ρ_e), and the power correlation (ρ_p) coefficients. One can express the complex signal correlation coefficient as [2]

$$\rho_s = \frac{E[V_1 V_2^*]}{\sqrt{E[V_1 V_1^*]E[V_2 V_2^*]}} \tag{1}$$

where V_1 and V_2 are the zero-mean complex voltages at the first and second antenna terminals, respectively, and $E[\,]$ is the expected value operator. The definitions of the envelope and power correlation coefficients found in [11] are as follows:

$$\rho_e = \frac{E[\sqrt{S_1}\sqrt{S_2}]}{\sqrt{E[\sqrt{S_1}\sqrt{S_1}]E[\sqrt{S_2}\sqrt{S_2}]}} \tag{2}$$

$$\rho_p = \frac{E[S_1 S_2]}{\sqrt{E[S_1 S_1]E[S_2 S_2]}} \tag{3}$$

where S_n represents the zero-meaned sequence of the power received over the nth antenna. In the literature, the most common reference to diversity performance is in terms of the envelope correlation although all three measurements of correlation are related. It is a widely held assumption that $|\rho_s|^2 \simeq \rho_e$ in a Rayleigh fading environment [11], [12] although negative values of ρ_e have been observed [13]. Both experimentally and analytically, it has been shown that $\rho_e = \rho_p$ for all practical purposes [11], [13].

B. Extraction of Multipath Behavior

The demeaning of the data before calculation of the correlation is important to remove slow fades resulting from propagation losses and, hence, not a function of multipath. During a dynamic measurement of the signals, as the distance and obstacles between the transmitter and receiver

vary, the overall strength of all the multipath components will experience similar variations simply due to the changing environment. This long-term or slow fading is not a function of multipath and should be ignored in the diversity computations. This is accomplished by extracting the *local* mean of the measured data before performing the correlation coefficient computations. By *local* mean, it is meant a relatively long-term moving average of the observed envelope. Two ways of demeaning the data have been used, and it has been seen that the different techniques will not yield the exact same result [14]. The conclusion in [14] is that when correlation data is presented, the processing technique used must also be specified in order to be able to make any inference between studies.

In this work, the slow fading is assumed to be a multiplication factor of the observed envelope. That is, letting $A_o(x)$ be the observed envelope, $m(x)$ the observed envelope *local* mean which contains the slow-fading information, and $A(x)$ the fast-fading envelope, we can relate these terms as

$$A_o(x) = m(x)A(x). \tag{4}$$

Using this assumption, one can extract the fast fading from the observed envelope by simply normalizing it with the *local* mean.

More care should be given to the issue of the observed envelope local mean. An expression for the local mean, which is just a long-term moving average, is

$$m(x) = \frac{1}{2L} \int_{x-L}^{x+L} A_o(\tau)\, d\tau. \tag{5}$$

One question that arises is what L should be used? For indoor propagation measurements, past work has used measurement lengths from 5 to 20 wavelengths to compute the local means [15], [16]. Data will be presented on the variation of the computed power correlation coefficient with the duration of the local mean, and it will be seen that the computed results are fairly insensitive to the exact value used.

The measured data was also seen to contain a very fast, but small ripple not associated with short-term multipath fading or path loss. This ripple is considered a measurement error, and it is believed to have been introduced in the digitizing process. To remove this error, a very short-term averaging was performed on the data. The number of data samples averaged to smooth the experimental noise was varied from one to nine, and no strong effect was observed on the computed correlation. For the correlation results shown in this work, a three-point short-term averaging was used for smoothing. Details on the effect the short-term averaging had on the computed correlations can be found in [17].

C. Power Correlation Coefficient Calculation

As discussed below in the experimental setup section, in these measurements the actual values recorded during the experiments were the power received, expressed in decibels relative to 1 mW (dBm), by each antenna. The recorded data were converted to milliwatts before the power correlation coefficients were computed. That is, the discretized power envelopes (S_n) were computed from the measured data as $S_n = 10^{P_n/10}$, where P_n is the recorded data (in dBm) on the nth channel. Before the recorded data were converted to a milliwatt scale, the short-term averaging was performed to remove the experimental noise since it was believed the noise was introduced in the digitizing of the received power in dBm.

The demeaning of the data was performed on the data in the millimeter scale. From the normalized power envelope sequences (S_n), the expression used to compute the power correlation coefficients was

$$\rho_p = \frac{\sum_{i=1}^{N} (S_1(i)-1)(S_2(i)-1)}{\sqrt{\left(\sum_{i=1}^{N} (S_1(i)-1)^2\right)\left(\sum_{i=1}^{N} (S_2(i)-1)^2\right)}} \tag{6}$$

where N is the number of discrete data points recorded during each test.

IV. Experimental Setup and Procedure

A diagram of the equipment setup used to conduct the correlation measurements of the proposed dual-antenna handset configurations is shown in Fig. 2. The transmitter for these tests consisted of a sweep oscillator (HP8350B sweep oscillator) connected to a $\lambda/2$ dipole antenna. The source was operated in single-frequency mode at 915 MHz. The source output power was adjusted to 17 dBm, and the reflection coefficient of the transmitting dipole was measured to be under -10 dB at the frequency of interest.

On the receiver end, the antenna geometries described in Section II were used as antennas 1 and 2. For example, when testing the handset shown in Fig. 1(a), the top-mounted helix would be antenna 1 and the back-mounted PIFA would be antenna 2. The outputs of these antennas were amplified (Avantek 0.5–2.0-GHz amplifiers) and then directed into separate spectrum analyzers (HP8592A spectrum analyzers). Preamplification of the signals was performed to increase the measurable fading range of the multipath signals. The spectrum analyzers were put in zero span mode and centered on 915 MHz for which the video output signals were proportional to the received power in dBm. The analog video output signals of the spectrum analyzers were then digitized and the data recorded on a personal computer. The digitizing rate used was approximately 72 samples per second per channel.

For each test run, the receiver was located in a typical laboratory room in the Engineering IV building on the University of California at Los Angeles (UCLA) campus while the transmitting antenna was moved along one of six predetermined paths at a constant speed. The paths were chosen such that there was no line-of-sight between the transmitter and receiver. Results from two of the original six paths are not included in this paper because their fading characteristics were considered corrupted. The fading probability distributions for the two paths eliminated from this paper differed considerably from expectations and the other four paths. One of the paths eliminated from this paper exhibited the presence of a dominant propagation path, and the

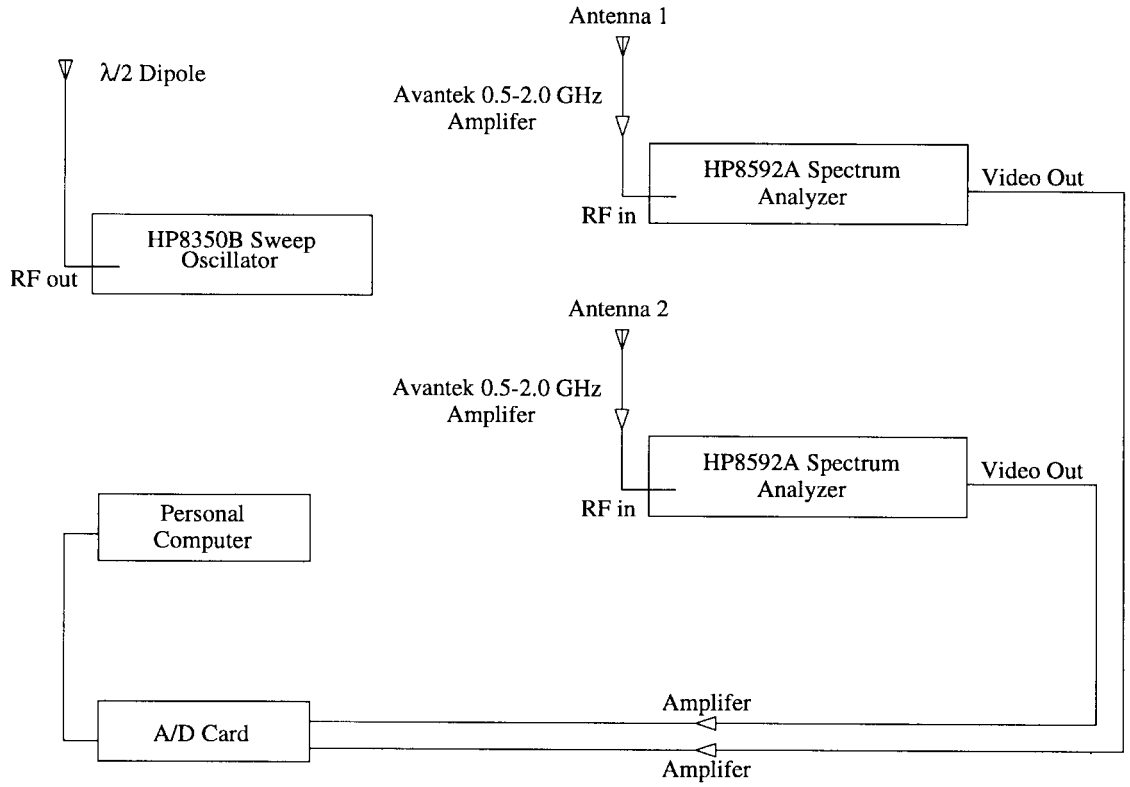

Fig. 2. Equipment setup for antenna diversity measurements. In the experiments conducted, the transmitter, which consisted of the sweep oscillator and the $\lambda/2$ dipole, was moved while the receiver remained stationary.

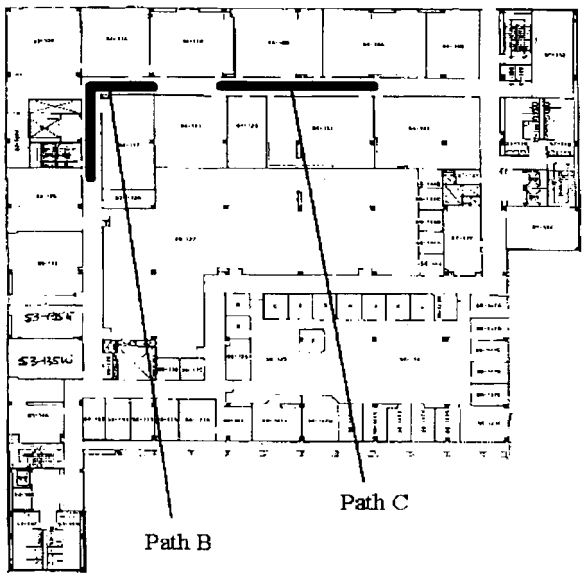

Fig. 3. Floor layout of the fifth floor of the Engineering IV building on the UCLA campus, with the test paths B and C indicated. The approximate floor dimensions are 67 m × 60 m.

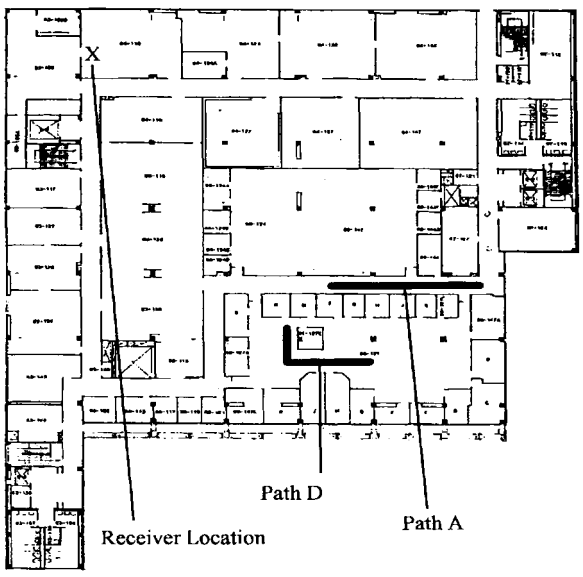

Fig. 4. Floor layout of the sixth floor of the Engineering IV building on the UCLA campus, with the test paths A, D, and the receiver location indicated. The approximate floor dimensions are 67 m × 60 m.

fading data from the other path eliminated from consideration experienced clipping of the deep fades by the noise floor of the experimental setup. Of the four paths considered most relevant, two were located on the same floor as the receiver (they will be referred to as paths A and D), and two were located on the floor below the receiver (they will be referred to as paths B and C). Figs. 3 and 4 indicate the four paths of interest in this paper. The Engineering IV building on the UCLA campus is a large office building of modern construction consisting of individual offices, large open laboratories, and cubical areas. The approximate floor dimensions are 67 m × 60 m. During each test run, the transmitter was moved approximately 0.5 m per second, and the time length of each test run was 30 s. For movement at 0.5 m per second and analog–digital sampling at

72 samples per second per channel, at 915 MHz this translates into approximately 50 samples per wavelength.

As mentioned, in these experiments the dual-antenna receiver remained stationary while the transmitter was moved. This scenario is opposite to that of actual interest since it is intended the user will move the dual-antenna transceiver and the base station will remain stationary. The experiments were conducted with the aforementioned procedure because logistically the dipole/sweep oscillator transmitter was easier to move compared to the dual-antenna handset/two spectrum analyzer/personal computer receiver setup. In the indoor scenario of interest in this study, both the base station and mobile unit are located in local environments exhibiting the same type of close proximity/uniformly distributed multipath scatterers. Thus, although the test procedure used does not exactly replicate the situation of interest, it is believed to be statistically similar.

In these experiments, the effect of the operator's presence on the diversity performance of the handsets was not included. In [7] and [18], FDTD computations indicated that close proximity of the operator's head to the radiating elements significantly affects the handset's far-field radiation, which should, in turn, affect the diversity performance of the dual-antenna configurations considered in this work. The sensitivity of the handset's radiation characteristics with respect to its exact location and orientation relative to a head made repeatability and comparison between separate data sets difficult. Because in this work it was intended to make relative comparisons between the different dual-antenna configurations, the operator's presence was excluded from the experiments. Additional comments on the effect of the operator's presence on diversity performance of these handsets are made in Section VI of this paper.

V. Experimental Results

A. Experimental Setup and Procedure Evaluation

For reference, initial diversity tests were performed with two vertically oriented dipole antennas. The instrumentation was set up as described in Section IV, with two dipoles used as antennas 1 and 2. Experiments were performed on the four test paths described in Section IV for dipole spacings of 0.06λ and 0.4λ (at 915 MHz). After testing the dual-dipole antenna configurations, the dual-antenna handsets described in Section II were tested. Fig. 5(a) is a plot of raw data recorded for test path A from one of the two side-mounted PIFA's on the handset illustrated in Fig. 1(b). In Fig. 5(a), both the long-term shadow/path-loss fading and short-term multipath fading can be seen. Fig. 5(b) is a plot of the same data segments after the local mean (calculated over a six-wavelength period) was extracted. Fig. 5(a) and (b) is representative plots of the observed fading behavior.

B. Fading Distributions

A common model for indoor short-term fading is that it follows either a Rician or Rayleigh distribution [19]. In a pure multipath environment, where many equal amplitude and uniformly distributed phase replicas of the transmitted signal arrive at the receiver, the short-term fading envelope will have a Rayleigh probability density function (PDF)

$$p(r) = \frac{r}{\sigma^2} \exp\left(-\frac{r^2}{2\sigma^2}\right) \tag{7}$$

where σ^2 is the mean signal power and $r^2/2$ is the short-term signal power. However, when there is line-of-sight, or at least a dominant specular component, the short-term fading envelope will have a Rician PDF

$$p(r) = \frac{r}{\sigma^2} \exp\left(-\frac{r^2 + r_s^2}{2\sigma^2}\right) I_o\left(\frac{r r_s}{\sigma^2}\right) \tag{8}$$

where I_o is the zero-order modified Bessel function of the first kind, σ^2 is the mean signal power, $r^2/2$ is the short-term signal power, and $r_s^2/2$ is the power of the dominant component. Note that the Rayleigh distribution is a special case of the Rician distribution when $r_s = 0$. A commonly used notation for the dominant to multipath signal power ratio for the Rician distribution [20] is

$$K = 10 \log \frac{r_s^2}{2\sigma^2} \quad \text{dB}. \tag{9}$$

As an example of the fading behavior experienced on the selected paths, consider the data collected with the two side-mounted PIFA handset configuration, shown in Fig. 1(b), for the four paths of interest. Figs. 6–9 contain plots of the cumulative distribution functions (CDF's) for the signal received by one of the dual PIFA's for data sets from each of the paths (the *local* mean used to normalize the data was computed over a six-wavelength region). Also, on each plot is the *best* fit to a theoretical CDF in addition to a true Rayleigh CDF for comparison purposes. The *best* fit to a theoretical CDF was determined in the minimum mean-squared error sense between the measured CDF's and true Rician CDF's for K values between -5 to 15 dB in steps of 0.5 dB. A true Rayleigh CDF was also used in the test. In [17], similar CDF plots are presented for all the data sets recorded. Table I lists the *best* K values computed for the four test paths of interest. Note that $K = -\infty$ denotes a pure Rayleigh distribution.

From Table I, it can be seen the paths of interest in this study exhibit strong multipath behavior (either a true Rayleigh or a Rician with a small value of K was the *best* fit). In a different set of experiments, the coherence bandwidths of the indoor channel at two locations on the paths of interest were measured to be less than 2 MHz. Details of this indoor coherence bandwidth study can be found in [17].

C. Computed Power Correlation Coefficients

Using (6), the power correlation coefficients for the data sets recorded in the experiments were determined. Table II lists the power correlation coefficients computed from the data sets for the dual-side-mounted PIFA handset recorded

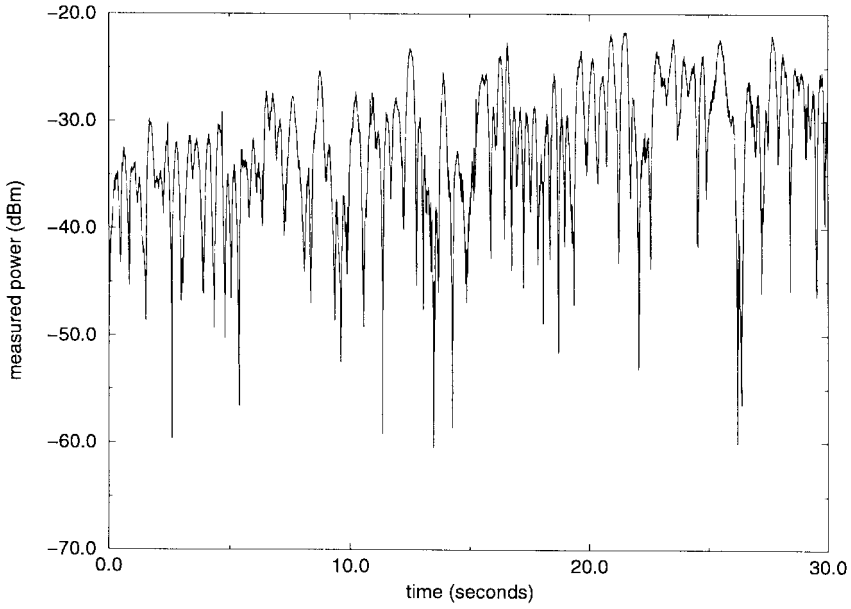

(a)

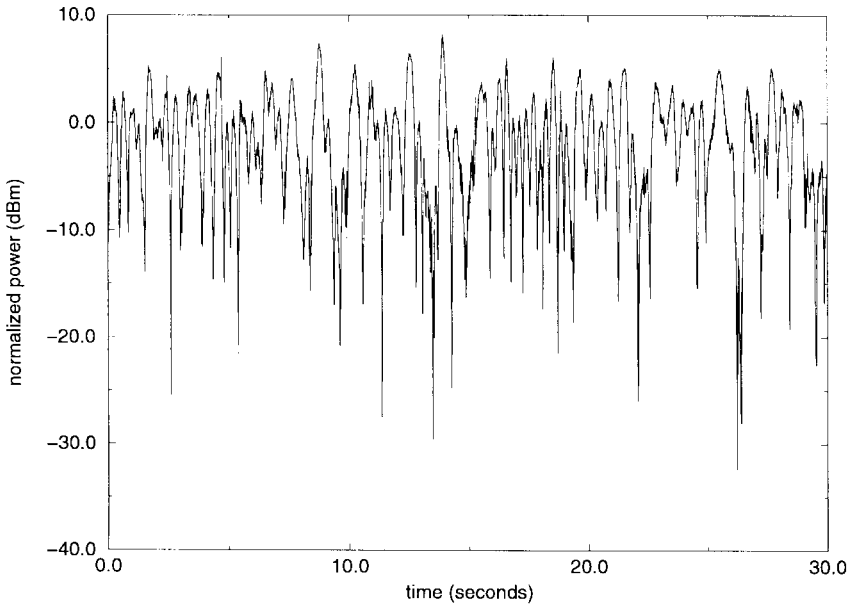

(b)

Fig. 5. (a) Recorded signal strength (at 915 MHz) for one of the two side-mounted PIFA's on path A. (b) Same data set as in (a) except demeaned by a six-wavelength *local* mean.

over the four paths of interest. In this table, the different columns represent different test paths, and the different rows correspond to the period used in the calculation of the *local* mean. The length used in the *local* mean determination was varied from approximately 1.5λ to 13.5λ. In [17], additional tables are presented for all the data sets recorded. From the data in Table II, it can be seen that the computed values of the correlation coefficient are fairly insensitive to the different demeaning periods used. Also note that negative values of ρ_p were recorded, which is inconsistent with the assumption $\rho_p = \rho_e \simeq |\rho_s|^2$, but has been previously observed experimentally [13]. Of all the negative correlation coefficient recorded, the largest number in absolute value was -0.0902, with most of the negative values being much closer to zero. These very small negative correlation values could potentially be an artifact of the finiteness and discreteness of the data sequences from which they were computed.

Table III lists the computed correlation coefficients for the five different dual-antenna configurations noted earlier on each of the four test paths of interest. The data shown in Table III assumes a six-wavelength demeaning length of the raw data. From Table III, one can see all three proposed dual-antenna handset designs achieve decorrelations approximately equal to that of two vertically orientated dipole antennas with 0.4λ of horizontal separation. Note that the reported decorrelation performances for the handsets were achieved

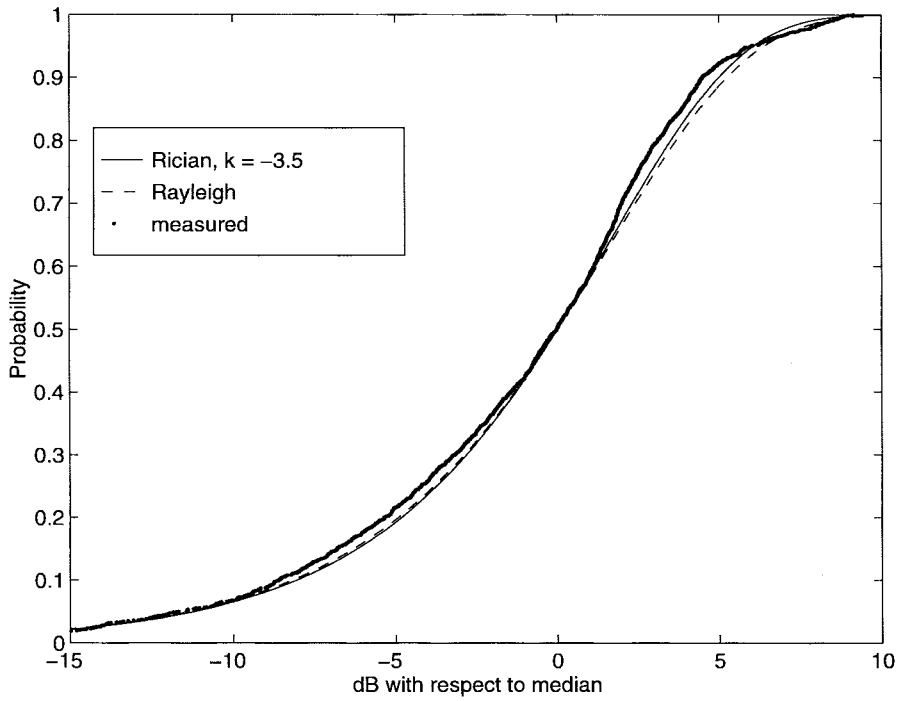

Fig. 6. Comparison of the measured *best*-fit Rician and Rayleigh CDF's for one of the two side-mounted PIFA's data sets recorded on path A.

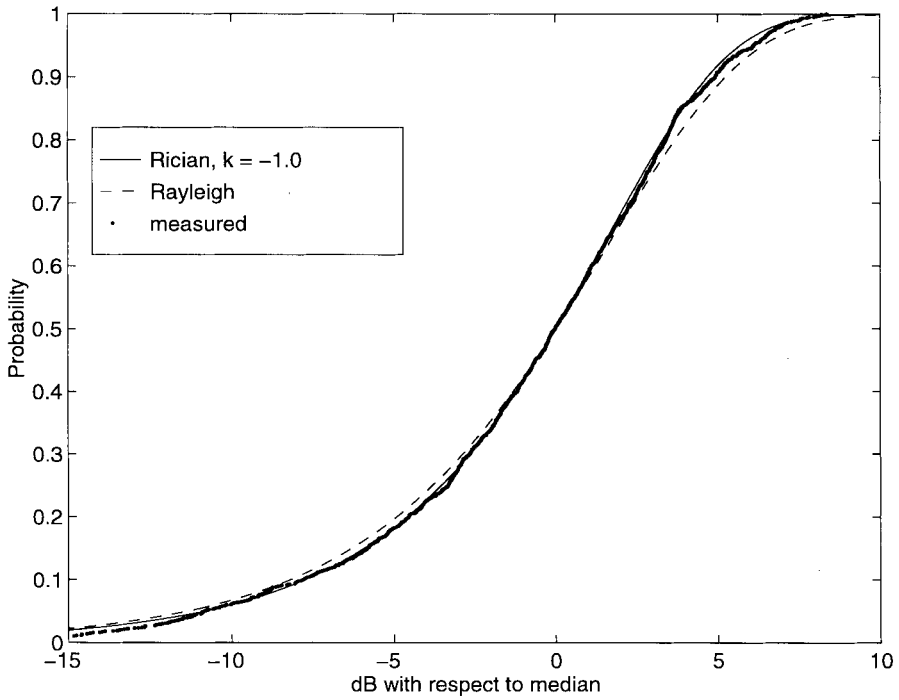

Fig. 7. Comparison of the measured *best*-fit Rician and Rayleigh CDF's for one of the two side-mounted PIFA's data sets recorded on path B.

with antenna separation of approximately 0.15λ for both the top-mounted helix/back-mounted PIFA and dual-side-mounted PIFA handsets and 0.45λ for the top-mounted helix and "flip" monopole handset.

In this work, the mean effective gains for the antennas on the proposed handsets were not measured. A complete benefit comparison of the proposed dual-antenna handsets relative to horizontally separated dipole antennas requires consideration of the mean effective gains of the radiating elements in addition to the antenna correlation. For the case of equal mean effective gains, it is known that in Rayleigh fading environments the majority of two-branch diversity gain can be obtained with branch decorrelations of 0.2 and less [1], [11]. Based on the values of the power correlation coefficient listed in Table III, the three proposed dual-antenna handsets achieve most of the theoretical two-channel diversity gain.

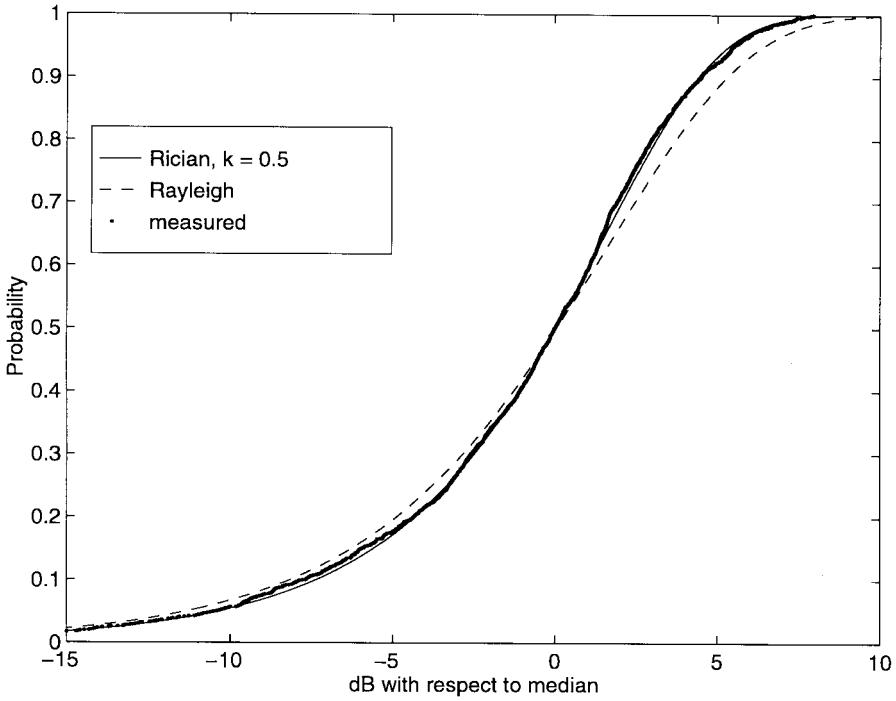

Fig. 8. Comparison of the measured *best*-fit Rician and Rayleigh CDF's for one of the two side-mounted PIFA's data sets recorded on path C.

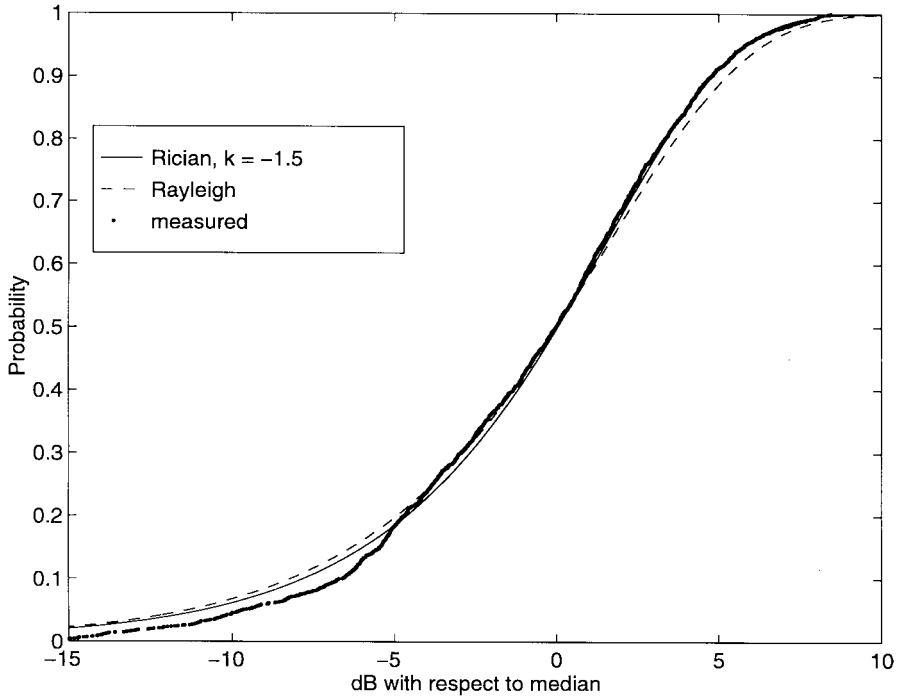

Fig. 9. Comparison of the measured *best*-fit Rician and Rayleigh CDF's for one of the two side-mounted PIFA's data sets recorded on path D.

VI. Operator Proximity Effects

As noted in Section IV, in these tests no operator was in close proximity to the handset under test. Computations have shown the operator's presence can significantly change the polarization and pattern of the far-field radiation [7], [18]. For the three dual-antenna configurations considered, each antenna's orientation with respect to the head and hand is different, thus, the depolarization and pattern distortion of each antenna's radiation caused by the head and hand would be different. It is believed this effect would not result in increased correlation coefficients for each of the three dual-antenna configurations considered. Note that although it is believed the operator's presence will not increase the elements' correlation, their mean effective gains will decrease due to absorption in the body tissue [7], [18]. Study of the effect the operator's presence has on the diversity performance of multiple-antenna configurations is left for future work.

TABLE I
BEST COMPUTED K VALUE FOR EACH OF THE MEASURED DATA SETS

Antenna Configuration	Path	K (dB)
0.06 λ dipole separation	A	-3.0
0.06 λ dipole separation	A	-2.5
0.06 λ dipole separation	B	-1.0
0.06 λ dipole separation	B	0.5
0.06 λ dipole separation	C	-∞
0.06 λ dipole separation	C	1.0
0.06 λ dipole separation	D	-∞
0.06 λ dipole separation	D	-1.0
0.4 λ dipole separation	A	-5.0
0.4 λ dipole separation	A	-3.5
0.4 λ dipole separation	B	-2.5
0.4 λ dipole separation	B	-2.0
0.4 λ dipole separation	C	-∞
0.4 λ dipole separation	C	2.0
0.4 λ dipole separation	D	-0.5
0.4 λ dipole separation	D	-1.5
side PIFAs	A	-1.5
side PIFAs	A	-3.5
side PIFAs	B	-1.0
side PIFAs	B	-2.0
side PIFAs	C	0.5
side PIFAs	C	-2.5
side PIFAs	D	-∞
side PIFAs	D	-1.5
top PIFA/"flip" monopole	A	-0.5
top PIFA/"flip" monopole	A	-∞
top PIFA/"flip" monopole	B	-0.5
top PIFA/"flip" monopole	B	1.0
top PIFA/"flip" monopole	C	-3.5
top PIFA/"flip" monopole	C	-2.5
back PIFA/helix	A	-2.5
back PIFA/helix	A	-1.0
back PIFA/helix	B	-0.5
back PIFA/helix	B	-∞
back PIFA/helix	C	0.5
back PIFA/helix	C	-5.0

TABLE II
POWER CORRELATION COEFFICIENTS CALCULATED FOR TWO SIDE-MOUNTED PIFA'S FOR THE FOUR TEST PATHS OF INTEREST AS A FUNCTION OF DEMEANING DISTANCE

	Test Path			
local mean length (λ)	A	B	C	D
1.5	-0.0920	-0.0458	0.1280	0.0265
3.0	-0.0161	-0.0647	0.0618	0.0432
4.5	-0.0374	-0.0182	0.0486	0.0512
6.0	-0.0215	0.0154	0.0578	0.0618
7.5	-0.0070	0.0168	0.0604	-0.0432
9.0	0.0015	0.0267	0.0293	-0.0530
10.5	-0.0057	0.0172	0.0550	-0.0656
12.0	-0.0180	0.0345	0.0462	-0.0701
13.5	-0.0182	0.0304	0.0538	-0.0796

VII. SUMMARY

In this paper, the diversity performance measurements of three proposed dual-antenna handset configurations were discussed: two side-mounted PIFA's, a back-mounted PIFA with a top-mounted helix, a top-mounted PIFA, with a "flip" monopole. The indoor 902–928-MHz propagation channel was studied, with both single-floor and floor-to-floor measurements in an office building of modern construction. Detailed descriptions of the experimental setup, procedures, and data processing were presented.

TABLE III
POWER CORRELATION COEFFICIENTS FOR THE PROPOSED ANTENNA CONFIGURATIONS. NA DENOTES DATA NOT AVAILABLE

Antenna Configuration	Path A	Path B	Path C	Path D
0.06 λ separated dipole	0.5667	0.5274	0.4186	0.5451
0.4 λ separated dipole	0.0608	0.1314	0.0462	0.0678
side PIFAs	-0.0215	0.0154	0.0578	0.0618
back PIFA/helix	0.0954	0.1088	0.0655	NA
top PIFA/"flip" monopole	-0.0451	0.1977	0.0894	NA

Indoor fading distributions of the observed signals were shown and seen to fit the Rician and Rayleigh models. Results were also presented on the issue of signal normalization and its effect on computed power correlation coefficients. It was observed that the calculations were fairly insensitive to the exact normalization period used.

As a point of reference for the diversity evaluation of the dual-antenna handsets, the diversity performance of two dipole antennas was also presented. The results illustrated all three proposed dual-antenna handsets have antenna decorrelation approximately equal to that of two vertically orientated dipoles with 0.4λ of horizontal separation. The data from these experiments indicate that the three proposed dual-antenna handset configurations achieve sufficient decorrelation to warrant their consideration for use in a diversity system.

ACKNOWLEDGMENT

The authors wish to thank R. A. Hoferer for his assistance in completing these experiments.

REFERENCES

[1] W. C. Jakes, *Microwave Mobile Communications*. New York: Wiley, 1974.
[2] W. C. Y. Lee, *Mobile Communications Engineering*. New York: Wiley, 1982.
[3] D. C. Cox, "Antenna diversity performance in mitigating the effects of portable radiotelephone orientation and multipath propagation," *IEEE Trans. Commun.*, vol. COM-31, pp. 620–628, May 1983.
[4] R. G. Vaughan and J. B. Andersen, "Antenna diversity in mobile communications," *IEEE Trans. Veh. Technol.*, vol. VT-36, pp. 149–172, Nov. 1987.
[5] Y. Yamada, Y. Ebine, and K. Tsunekawa, "Base and mobile station antennas for land mobile radio systems," *IEICE Trans.*, vol. 74, pp. 1547–1555, June 1991.
[6] Y. Yamada, K. Kagoshima, and K. Tsunekawa, "Diversity antennas for base and mobile stations in land mobile communications systems," *IEICE Trans.*, vol. 74, pp. 3202–3209, Oct. 1991.
[7] M. A. Jensen and Y. Rahmat-Samii, "Time-domain finite-difference methods in electromagnetics: Applications to personal communications," Tech. Rep. ENG-95-113, Univ. Calif., Los Angeles, Oct. 1994.
[8] ——, "Performance analysis of antennas for hand-held transceivers using FDTD," *IEEE Trans. Antennas Propagat.*, vol. 42, pp. 1106–1113, Aug. 1994.
[9] R. G. Vaughan, "Polarization diversity in mobile communications," *IEEE Trans. Veh. Technol.*, vol. 39, pp. 177–186, Aug. 1990.
[10] J. Lemieux, M. S. El-Tanany, and H. M. Hafez, "Experimental evaluation of space/frequency/polarization diversity in the indoor wireless channel," *IEEE Trans. Veh. Technol.*, vol. 40, pp. 569–573, Aug. 1991.
[11] J. N. Pierce and S. Stein, "Multiple diversity with nonindependent fading," in *Proc. IRE*, Jan. 1960, pp. 89–104.
[12] M. T. Feeney and J. D. Parsons, "Cross-correlation between 900 MHz signals received on vertically separated antennas in small-cell mobile radio systems," *Proc. Inst. Elect. Eng.*, vol. 138, pt. I, pp. 81–86, Apr. 1991.
[13] P. C. F. Eggers, J. Toftgård, and A. M. Oprea, "Antenna systems for base station diversity in urban small and micro cells," *IEEE J. Select. Areas Commun.*, vol. 7, pp. 1046–1057, Sept. 1993.
[14] N. L. Scott and R. G. Vaughan, "The effect of demeaning on signal envelope correlation analysis," in *PIMRC'93,* Yokohama, Japan, Sept. 1993, pp. 583–587.

[15] S. Y. Seide and T. S. Rappaport, "914 MHz path loss prediction models for indoor wireless communications in multifloored buildings," *IEEE Trans. Antennas Propagat.*, vol. 40, pp. 207–217, Feb. 1992.
[16] T. S. Rappaport and S. Sandhu, "Radio-wave propagation for emerging wireless personal-communication systems," *IEEE Antennas Propagat. Mag.*, vol. 36, pp. 14–24, Oct. 1994.
[17] J. S. Colburn, M. A. Jensen, G. J. Pottie, and Y. Rahmat-Samii, "Indoor ISM band propagation/diversity measurements," Tech. Rep. ENG-95-133, Univ. Calif., Los Angeles, Aug. 1995.
[18] M. A. Jensen and Y. Rahmat-Samii, "Em interaction of handset antennas and a human in personal communications," *Proc. IEEE*, vol. 83, pp. 7–17, Jan. 1995.
[19] D. Parsons, *The Mobile Radio Propagation Channel*. New York: Halsted, 1992.
[20] J. P. Castro, "Data transmission over land mobile satellite channels," *Space Commun.*, vol. 10, pp. 119–131, 1992.

Joseph S. Colburn (S'90) received the B.S.E.E. degree (*summa cum laude*) from the University of Washington, Seattle, in 1992 and the M.S.E.E. degree from the University of California, Los Angeles, in 1994. He is currently working toward the Ph.D. degree at the University of California, Los Angeles.

He is also currently with TRW Space and Electronics Group, Redondo Beach, CA. His research interests include radiation and propagation issues in wireless communications and related topics in numerical electromagnetics. Other relevant experience includes internships at the Department of Energy NORCUS program, US West NewVector, University of Washington Electromagnetics and Remote Sensing Laboratory, and Sandia National Laboratories.

Yahya Rahmat-Samii (S'73–M'75–SM'79–F'85) received the M.S. and Ph.D. degrees in electrical engineering from the University of Illinois, Urbana-Champaign.

He is a Professor of Electrical Engineering at the University of California, Los Angeles. He was a Senior Research Scientist at NASA's Jet Propulsion Laboratory, California Institute of Technology, Pasadena, before joining the University of California. He was a Guest Professor at the Technical University of Denmark (TUD) in the summer of 1986. He has also been a Consultant to many aerospace companies. He has authored and coauthored over 400 technical journal articles and conference papers and has written 14 book chapters. He is the coauthor *Impedance Boundary Conditions in Electromagnetics*, which was published in 1995. He is also the holder of several patents. His research contributions cover a diverse area of electromagnetics, antennas, measurement and diagnostics techniques, numerical and asymptotic methods, and satellite and personal communications.

Dr. Rahmat-Samii has received numerous NASA and JPL Certificates of Recognition. In 1984, he was the recipient of the prestigious Henry Booker Award of URSI. In 1992 and 1995, he was the recipient of the Best Application Paper Award (Wheeler Award) for papers published in the 1991 and 1993 IEEE TRANSACTIONS ON ANTENNAS AND PROPAGATION. He is a Member of Commissions A, B, and J of USNC/URSI, AMTA, Sigma Xi, Eta Kappa Nu, and the Electromagnetics Academy. He is listed in *Who's Who in America*, *Who's Who in Frontiers of Science and Technology*, and *Who's Who in Engineering*. He was the 1995 President of the IEEE Antennas and Propagation Society. He was appointed an IEEE Antennas and Propagation Society Distinguished Lecturer and presented lectures internationally. He was elected as a Fellow of IAE in 1986. Currently, he is a Member of the Strategic Planning and Review Committee (SPARC) of IEEE. He has been the Guest and Plenary Session Speaker at many national and international symposia. He was one of the Directors and Vice President of the Antennas Measurement Techniques Association (AMTA) for three years. He has been Editor and Guest Editor of many technical journals and book publication entities, including Co-guest Editor of a Special Issue on Wireless Communications of the IEEE TRANSACTIONS ON ANTENNAS AND PROPAGATION, which was published in June 1998. He was also a Member of the University of California's Graduate Council.

Michael A. Jensen (S'93–M'95) received the B.S. (*summa cum laude*) and M.S. degrees in electrical engineering from Brigham Young University (BYU), Provo, UT, in 1990 and 1991, respectively, and the Ph.D. degree in electrical engineering at the University of California, Los Angeles, in 1994.

From 1989 to 1991, he was a Graduate Research Assistant in the Lasers and Optics Laboratory at BYU. From 1991 to 1994, he was a Graduate Student Researcher at the Antenna Laboratory at the University of California. Since 1994, he has been an Assistant Professor in the Electrical and Computer Engineering Department, BYU. His main research interests include radiation and propagation for personal communications, numerical electromagnetics, optical fiber communication, and implementation of finite-difference schemes on massively parallel computer architectures.

Dr. Jensen received a National Science Foundation Graduate Fellowship in 1990. He is a Member of Eta Kappa Nu and Tau Beta Pi.

Gregory J. Pottie (S'85–M'89) received the B.Sc. degree in engineering physics from Queen's University, Kingston, Ont., Canada, in 1984 and the M.Eng. and Ph.D. degrees from McMaster University, Hamilton, Ont., in 1985 and 1988, respectively.

From 1989 until 1991, he worked in the Transmission Research Department, Codex/Motorola, on projects including high-speed digital subscriber lines and coding and equalization schemes for voice-band modems. He is presently an Associate Professor in the Electrical Engineering Department, University of California, Los Angeles. His research interests include channel coding and systems design for personal communication transceivers and wireless distributed sensor networks.